Lasers in Manufacturing Conference 2021

Impact of sulphur content on spattering and weld seam shape in steel specimens using modified side-gas application technique

Goran Jovic[a,d,*], Axel Bormann[a], Johannes Pröll[b], Thomas Niendorf[c], Stefan Böhm[d]

[a]*Robert Bosch GmbH, Manufacturing Center of Competence Laser Welding, Am Börstig 2, 96052 Bamberg, Germany*
[b]*Robert Bosch GmbH, BaP/TEF1.2 – Laser Material Processing and Joining Technology, Am Börstig 2, 96052 Bamberg, Germany*
[c]*Institute of Materials Engineering – Metallic Alloys, University of Kassel, Mönchebergstr. 3, 34125 Kassel, Germany*
[d]*Department for Cutting and Joining Manufacturing Processes, University of Kassel, Kurt-Wolters-Str. 3, 34125 Kassel, Germany*

Abstract

Laser welding experiments have been carried out using stainless steel specimens (1.4003/1.4005) with different sulphur contents (S1:10ppm, S2:210ppm, S3:2770ppm). A parameter for spatter control, the capillary widening ratio mainly affected by the side-gas jet is considered. This value can be controlled by welding speed, laser power and side-gas pressure. Decreasing the sulphur content resulted in (1) a shift of the humping threshold to higher side-gas pressure and (2) an increase in weld seam bulge while decreasing spatter quantity at the same time. For S1 and S2, aspect ratios of R>3 were achieved while spattering could not be detected by high speed imaging at 2000 fps. By increasing the welding speed from 1.5m/min to 3.0m/min and a simultaneous adaption of laser power, differences in spattering and weld seam shape between S1 and S2 were minor, indicating that higher melt pool velocities acting in welding direction dominate the surface tension driven effects.

Keywords: Side-gas application, spatter reduction, weld shape modification, surface tension;

1. Introduction

The scope of laser welding applications is limited by the ejection of melt droplets from a weld pool (=spatter) which are typically formed within the deep penetration regime, Kaplan and Powell, 2011. Even though spattering has been studied on a large-scale, its underlying formation mechanisms are not yet fully understood due to a strong interdependency of the forces acting in and around the capillary and the weld pool. It is assumed that rather small and continuously ejected spatter, with dimensions being at least one order of magnitude lower than the corresponding weld pool dimensions, are controlled by a shearing force, which the metal vapor directly exerts on the surrounding capillary wall, Katayama et al., 2009. However, according to the calculations and measurements carried-out by Volpp, 2017, these spatter phenomena rather involve the superposition of the vapor pressure with other pressure and flow components in the weld pool. In addition,

* *Corresponding author. Tel: +49-951-1811281 .*
E-mail address: goran.jovic@de.bosch.com

bigger and more irregular ejections, with sizes being in the order of magnitude of the weld pool dimensions may result from keyhole instabilities itself, Heider et al., 2013. Other spatter phenomena include elongated melt volumes around the capillary opening arising perpendicularly to the specimen surface. Depending on their upward momentum, such melt columns can either detach as a whole, decompose into smaller spatter or backdrop to the weld pool, Katayama et al., 2011, Nakamura et al., 2015. Moreover, droplets re-entering the optical beam path can absorb the laser radiation once again resulting in other spatter or additional instabilities, Zhang et al., 2013, Da Silva et al., 2021. It is obvious that melt ejections are very versatile in terms of their appearance and subjected to multidimensional formation mechanisms. Eventually, Kaplan and Powell, 2011, described the condition for spatter formation using the following simplified equation:

$$\frac{1}{2} \cdot \rho_m \cdot u_m^2 = \frac{\sigma}{R} \tag{1}$$

According to this equation, melt droplets can detach from the weld pool if the stagnation pressure inside a local melt volume (left) exceeds its corresponding pressure due to surface tension (right). The basic impact of surface tension during laser welding, e.g. of surface active elements such as sulphur or oxygen, has already been studied for example by Ribic et al., 2011. Furthermore, it was concluded that surface tension driven effects are only effective up to a certain flowing velocity within the weld pool, which is directly related to the welding velocity, Fuhrich, 2005. Related to Eq. 1 it is expected that surface tension may affect spatter formation. Nevertheless, to the best of our knowledge, we did not find any empirical studies describing the correlation of surface tension and spattering so far.

A strong spatter reduction, e.g. by the application of a side-gas jet, Kamimuki et al., 2002, Fabbro et al., 2006, welding under vacuum, Gao et al., 2017, Abe et al., 2014, the use of superimposed beam intensity distributions, Speker et al., 2018, Jarwitz et. al, 2019, the use of beam oscillation, Sommer et al., 2019 or defocusing and/or the inclination of the laser beam, Weberpals, 2010, Kawahito et al., 2016, also involved one or more of the following process observations:

- Modification of capillary shape
- Reduction of weld pool volume (at the capillary front wall)
- Reduction of capillary and weld pool fluctuations
- Suppression of vapor plume (fluctuations)

Due to its cost-efficiency and due to the fact of exhibiting all four of the upper process characteristics, the side-gas method, first presented by Kamimuki et al., 2002, gained quite some popularity in recent years. In Jovic et al., 2019 and Jovic et al., 2020, when carrying-out lap-joint welds on martensitic steel samples with S < 100 ppm for both, the upper and lower joining partner, a significant spatter reduction could be observed as well as strong weld seam modifications (i.e. bulge formations). The latter was directly dependent on the side-gas pressure and the welding velocity. Increasing the welding velocity contributed to the reduction of the bulge formation. Exluding the center-gas flow (side-gas flow only) decreased the weld seam bulge as well. At the same time, spattering was increased. Therefore it was assumed that the processing zone could not sufficiently be shielded against the atmosphere by the sole side-gas supply. Furthermore, based on the optical appearance of the weld seam, it was concluded that oxygen was dissolved into the weld pool, significantly modifying the surface tension of the melted metal. Within other studies it was shown that the impact of a sole side-gas on the weld shape (even compared to no gas supply at all), can be neglected for higher welding velocities between 8 m/min and 16 m/min, Schmidt et al., 2019 and Schmidt et al., 2020. Yet, spattering could also be reduced by more than 90 %.

The aim of this paper is to discuss the contribution of surface tension to spatter formation within deep penetration welding as well as to the formation of spatter free regimes caused by a modified side-gas application. In order to impact on the surface tension of the melt within welding, steel specimens with a wide range of sulphur (S) contents were used for this study.

2. Methodology

According to the schematic in Fig. 1 (a), a continuous wave (cw) disk laser (TruDisk 1000, TRUMPF Laser- und Systemtechnik GmbH) with a maximum power of 1 kW, a wavelength of 1030 nm and a beam parameter product (BPP) of 2mm·mrad was used for the experiments. The beam was delivered by an optical fiber with an inner core diameter of 100 µm through a 100 mm collimation optics to a focusing optics with a focal length of 300 mm. Therefore, a calculated beam diameter of 300 µm in the focal plane with a calculated Rayleigh length of 5.625 mm could be realized.

Table 1. Chemical composition of welding specimens analyzed by optical emission spectrometry (OES), combustion technique (Leco CS-744) and hot gas extraction (Leco NO-736)

Specimen	Fe + others (wt.%)	C	Cr	Ni	Mo	Mn	Si	Al	S (ppm)	O	N	P
1.4003-S1	Bal.	0.039	11.30	0.36	0.08	1.03	0.45	0.009	10	25	98	190
1.4003-S2	Bal.	0.031	11.85	0.44	0.33	1.04	0.64	-	210	17	138	200
1.4005-S3	Bal.	0.024	12.06	0.15	0.31	0.86	0.72	-	2770	48	118	230

Weld trials were carried-out on round stainless steel specimen with a diameter of 5.9 mm. The specimen rotation was set to 350°. Thereby the start and end of weld seam solidification could be analysed by optical microscopy. The chemical compositions of the different EN 1.4003/1.4005 stainless steel specimens used within this study are listed in Table 1. The welding and process gas parameters are listed in Table 2.

Table 2. Welding and process-gas parameters

Parameter	Value(s)	Unit
Welding velocity	1.5, 3.0	m/min
Laser power	500 - 975	W
Focal diameter	300	µm
Focal position	0	mm
Process gas type	Nitrogen	-
Center-gas nozzle diameter	8	mm
Center-gas nozzle distance	12	mm
Center-gas nozzle angle	30	°
Center-gas volume flow	30	l/min
Side-gas nozzle diameter	0.8	mm
Side-gas nozzle distance	5	mm
Side-gas nozzle angle	50	°
Side-gas pressure	0 - 9	kPa

A detailed set-up of the two gas nozzles/flows relative to the capillary opening is depicted in Fig. 1 (b). While the laser beam is fixed in place and the rotational direction of the specimen is clockwise, both the side- and center-gas flow are pointed to the capillary front wall. The angle between the side-gas nozzle axis and the x-axis is defined as the side-nozzle angle. The nozzle distance refers to the minimal distance between the intersection point laser/material and the nozzle axis. Based on the parameters used in Kamimuki et al., 2002, the side-gas nozzle diameter was defined in a way to be approximately three times the focal diameter. The side-gas pressure was controlled by adjusting the flow rate through a mass flow meter. This parameter refers to the stagnation pressure at the theoretical capillary opening resulting from the side-gas jet. Based on Kamimuki et al., 2002, a specific sample was produced to measure the side-gas pressure at different flow rates.

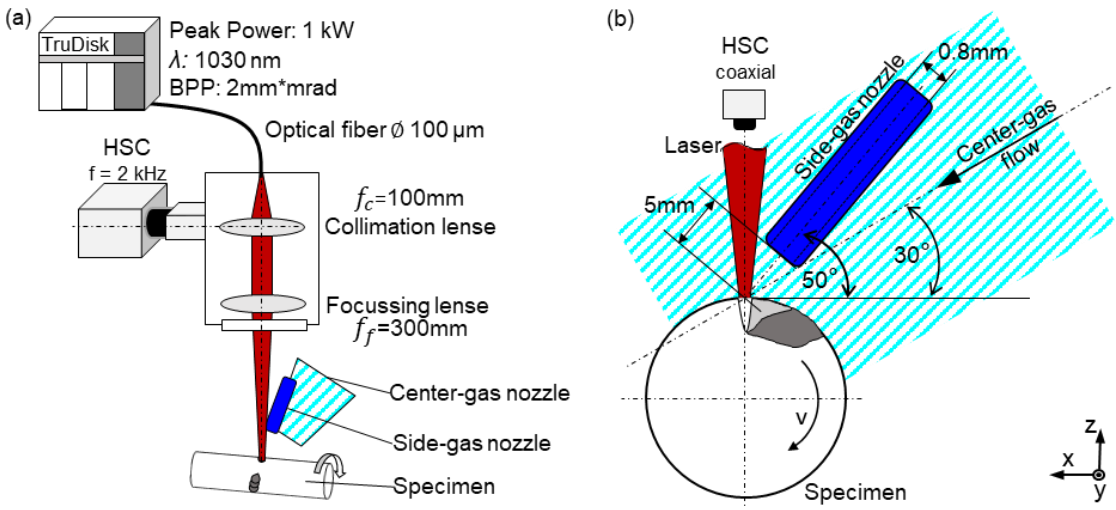

Fig. 1. Experimental system technology (a) and detailed set-up of the two gas nozzles/flows relative to the capillary opening (b).

A high-speed camera (HSC) was mounted coaxially to the laser beam axis, in order to observe spattering in a 2D-plane. The region of interest was approx. 20 x 20 mm and the frame rate was set to 2 kHz. This was estimated to be sufficient for spatter capturing and considering that spatter velocities in general do not exceed 10 m/s for steel applications as described by Kaplan and Powell, 2011. An evaluation algorithm was developed in *Python* based on the computer vision library *OpenCV.* Each high-speed recording was processed two times. In a first iteration it was distinguished between ‘static’ objects (e.g. vapor plume, reflections) and ‘dynamic’ objects (e.g. spatter). In a second iteration ‘static’ objects were masked while ‘dynamic’ objects were tracked based on an optical flow (Lukas-Kanade method) and additional logic. However, several disturbance factors depending on the laser process and the specimen itself were identified (e.g. moving reflections, overlapping bright spots within one frame). Therefore, spatter counts were constantly cross-checked half-manually by stacking a defined number of frames and counting spatter within the stacked images. Especially, for low spatter counts (≤ 10-20 per weld) with optimized side-gas process, this was the most robust way for spatter evaluation. Also, the instationary conditions during the first 3 mm of weld track have not been considered.

3. Results and Discussion

3.1. Reference processes without side-gas application

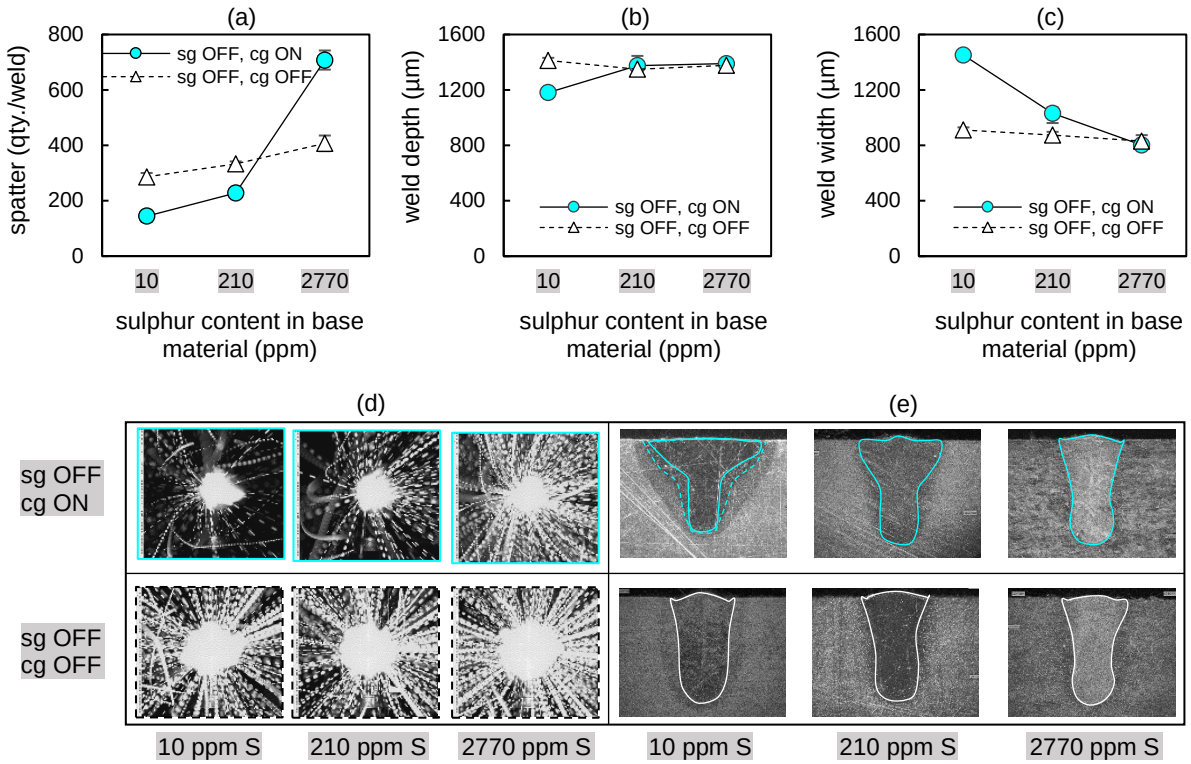

Fig. 2. Spatter quantity per weld seam (a), weld depth (b), weld width at specimen surface (c), superimposed images (d) and weld seam cross-sections (e) as a function of sulphur content within base material and process gas configuration (sg=side-gas, cg=center-gas). Welding velocity v = 1.5 m/min, laser power P = 600 W. N = 3.

In order to investigate the impact of surface tension driven effects on spattering and weld seam formation, the total spatter quantity per weld seam, the weld depth, and the weld width at the specimen surface have been analysed for two different process gas configurations and three different levels of sulphur content within the base material (Fig. 2). The side-gas (sg) was turned off while the center-gas (cg) was varied between off- and on-mode. The welding velocity and the laser power were kept constant at 1.5 m/min and 600 W, respectively. With the use of a center-gas flow (sg OFF, cg ON), spattering increased severely by increasing the sulphur content from 10 to 2770 ppm (Fig. 2 a). Once no process gas was used (sg OFF, cg OFF), the impact of sulphur content on spatter formation is weakened, which is also visualized by the superimposed images of the total welding process (Fig. 2 d). The images at 2770 ppm sulphur convey the impression that spattering is lower with the use of a center-gas, compared to no use of process gas at all. However, it is important to note that for the former configuration, smaller but more frequent spatter have been detected. Furthermore, the weld depth was around 1350 – 1400 µm for all parameter combinations except for 10 ppm sulphur and sg OFF, cg ON where it was about 200 µm lower (Fig. 2 b). Finally, the nail-head formation – expressed by the weld width at the specimen surface in Fig. 2 (c) and (e) – provided additional insight into the process. At sg OFF, cg ON the

nail-head shape decreased with increasing sulphur content while at sg OFF, cg OFF the weld width was not significantly affected. Considering the results from e.g., Su et al., 2005, it is assumed that the weld pool surface will be completely covered with surface active elements above approximately 500 ppm sulphur or oxygen within the base material. Even though the interaction between sulphur and oxygen is unclear, it is very likely that for the configuration sg OFF, cg ON and 2770 ppm sulphur, the melt pool surface is saturated with sulphur, while at sg OFF, cg OFF it may be saturated with oxygen and/or sulphur. Both elements indicate to have a similar impact on the surface tension, which is why all four 'saturated' weld seam shapes show a strong resemblance. It can be concluded that the welding results for spatter and weld seam formation can be affected by sulphur content within the base material given that the processing zone is shielded against the oxygen diffusion from the atmosphere. Therefore, the reference welding process was set to the application of a center-gas.

In Fig. 3, the total spatter quantity per weld seam is depicted as a function of different sulphur contents for various laser power and two different welding velocities based on the use of center-gas flow. For 10 ppm and 210 ppm sulphur, increasing the laser power leads to a steady increase of the spatter counts while at 2770 ppm sulphur, maximum spatter counts do not correspond to the use of maximum laser power. The latter can be explained by considering the spatter size since individual spatter dimensions appeared bigger with higher laser power in the superimposed images (not shown here). For this reason, it is assumed that it is rather the total ejected spatter volume, which is controlled by the laser power. It is remarkable that the average difference between the spatter quantities at 10 ppm S and 210 ppm sulphur is significantly reduced from 56% to 7% by increasing the welding velocity from 1.5 m/min to 3.0 m/min. This trend was equally observed for the weld depth and weld width (not shown here). Overall, these results suggest that surface tension driven spatter formation is dominated by the weld pool dynamics towards higher welding velocities. Within previous studies this was only validated for the weld seam formation itself (s. Section 1).

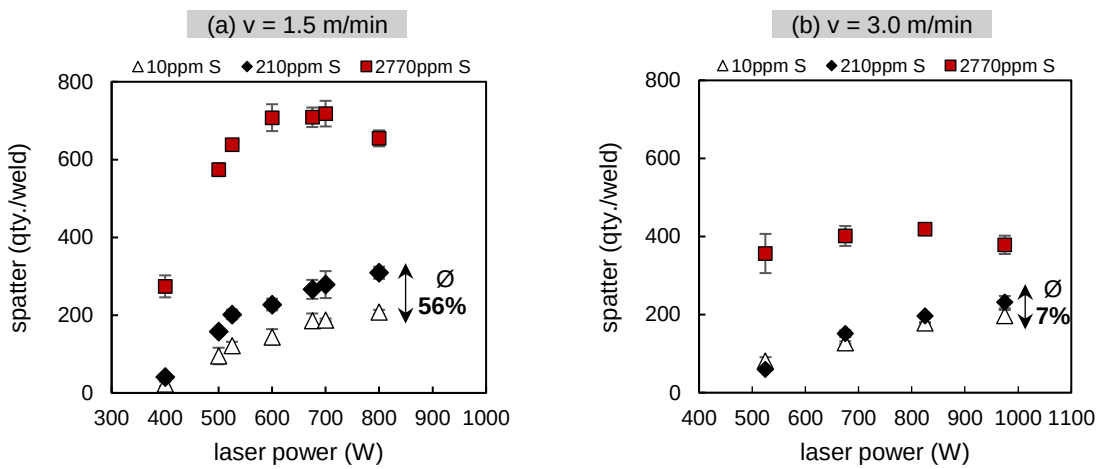

Fig. 3. Spatter quantity per weld seam as a function of laser power, sulphur content within base material and welding velocity with the use of center-gas. Increasing the welding velocity decreases the impact of sulphur content. N = 3.

3.2. Spatter suppression and weld seam modification with side-gas application

In Fig. 4 the total spatter quantity per weld seam is depicted as a colored contour plot as a function of side-gas pressure and laser power for two different welding velocities and three different sulphur contents. The data at a side-gas pressure of 0 kPa is representative for the process without side-gas (center-gas flow only). The black domains are representative of parameters where spatter were either completely suppressed or where only a couple of random spatter have been detected. At v = 1.5 m/min and 10 ppm sulphur, the application of a side-gas pressure of 7 kPa leads to a strong bulge formation (Fig. 4 a). Also, spattering could be reduced to 0, compared to about 150 spatter per weld for the reference process (0 kPa). This observation is comparable to previously presented welding results, whereby different steel types were welded in a lap-joint with S < 100 ppm for both joining partners, Jovic et al., 2020. As the sulphur content is increased to 210 ppm, the bulge formation is much less pronounced (Fig. 4 b). Spattering also shifted to the boundary between the black/purple domain and the weld seam was right at the humping threshold. It is worth noting that the threshold was set as soon as one single hump formation was detected within one of the N=4 samples. Severe humping was only observed between 8 – 9 kPa. Yet, a general trend of shifting the humping threshold towards higher side-gas pressure by decreasing the sulphur content becomes apparent.

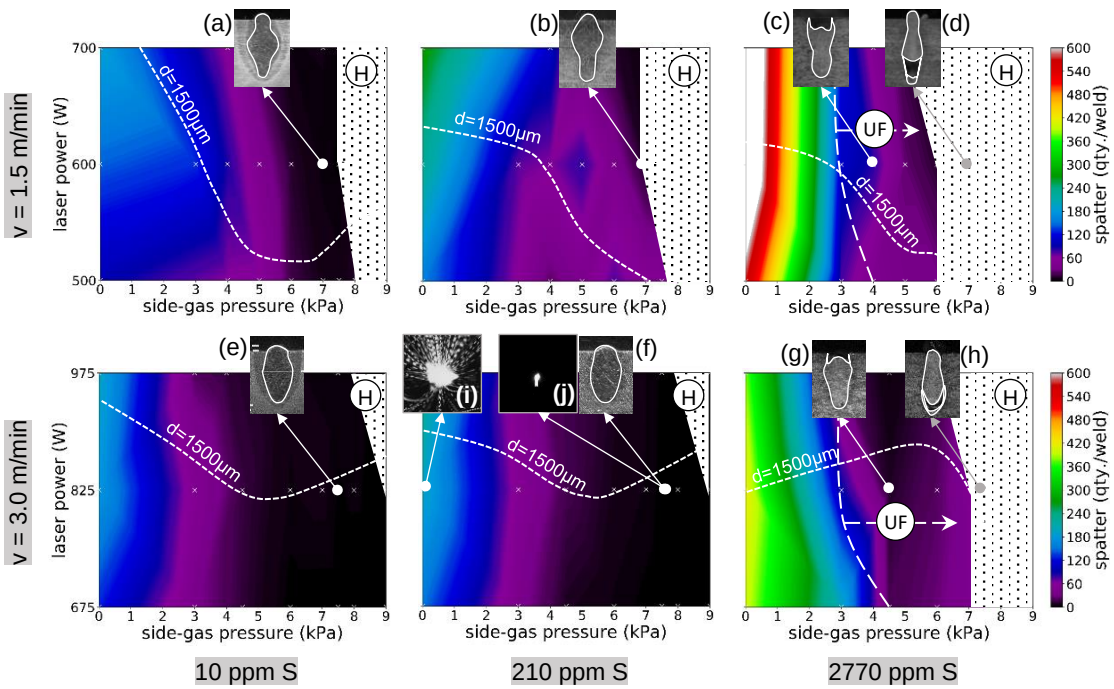

Fig. 4. Spatter quantity per weld as a function of welding velocity, laser power and side-gas pressure (Reference w/o side-gas = 0 kPa). Isoline for a weld depth of 1500 µm (dashed), Humping-Regime (H), Underfill-Regime (UF). Exemplary weld seam cross-sections (a)-(h). Exemplary superimposed images w/o side-gas (i) and w/ side-gas (j). N = 3 - 4. Total number welds ~ 400.

At v = 1.5 m/min and 2770 ppm sulphur, a rather big region of underfilled weld seams (Fig. 4 c) followed by a big region of humping (Fig. 4 d) can be observed. Therefore, the region with significantly reduced spattering combined with acceptable weld seam quality is very small (e.g. 3 kPa and 500 W). Finally, the contour plots have been overlayed by the isolines for a weld depth of 1500 µm. In this way, it can be implied, that the weld

depth is also strongly dependent on the sulphur content within the side-gas application at v = 1.5 m/min. Overall, these results suggest that the surface tension driven effects can also be effective once an additional side-gas is applied to the center-gas.

At v = 3.0 m/min for both 10 ppm and 210 ppm sulphur (Fig. 4) not only spattering but also the weld depth (isolines) and the weld shape (Fig. 4 e-f) as well as the humping threshold show very similar behaviour. The domain of minimal spattering (black) is significantly increased compared to v = 1.5 m/min at similar weld depths (e.g. 1500 µm). By comparing the superimposed image at a reference process (Fig. 4 i) and the superimposed image at a side-gas pressure of 7.5 kPa (Fig. 4 j) it is obvious that the side-gas application suppresses spatter formation as well as vapor plume formation. However, at 2770 ppm sulphur, once again a relatively big region of underfill and humping was observed.

It can be concluded that by increasing the welding speed less pure specimen can be used in order to achieve good weld seam quality and high penetration with minimal spattering. However, as described in section 1, it is assumed that above approximately 500 ppm sulphur (or oxygen), the process is dominated by the saturation of the weld pool surface with at least one of these surface active elements.

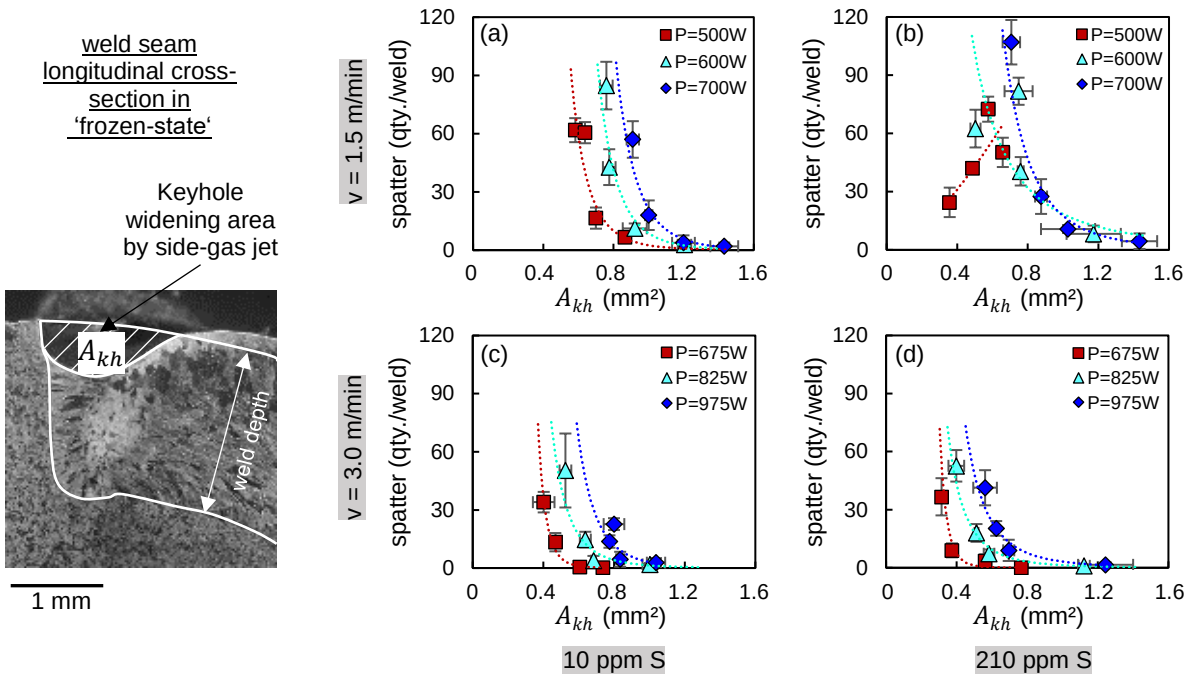

Fig. 5. Spatter quantity per weld seam as a function of capillary widening ratio, expressed by measuring the capillary widening area within longitudinal cross-sections at the weld seam centre-plane. By instantenously turning off the laser power while keeping the side-gas and feed rate active, each weld seam was put into so-called 'frozen-state'. N = 3.

In Fig. 5 a parameter for spatter control is introduced representing the keyhole widening ratio during welding induced by the side-gas jet. First, the weld seam was 'frozen', by instantaneously turning-off the laser power while keeping the side-gas and feed rate active. Second, by performing longitudinal cross-section cuts at the weld seam centre-plane, the area of the capillary widening A_{kh}, which in turn is controlled by the side-gas pressure, laser power and welding velocity could be measured by optical microscopy. It is shown that spattering decreases in some way exponentially with increasing A_{kh} (Fig. 5 a-d). Also, the data indicate that A_{kh} is increased towards higher laser power and that at constant A_{kh}, higher laser power leads to higher

spatter counts. Only at v = 1.5 m/min, 210 ppm sulphur (Fig. 5 b) and towards lower laser power a couple of outliers have been observed. Therefore, a closer analysis of the location of spatter detachment (e.g. capillary front-, side-, rearwall) is proposed for subsequent studies. The aim for future work is also to develop a model for the spatter threshold condition based on the input parameters such as laser power, welding velocity and side-gas pressure. It is proposed to link the model also to the weld seam characteristics such as weld depth and weld width.

4. Conclusion

In this study it could be demonstrated that the surface tension – expressed by the amount of sulphur within the base material – can lead to a significant impact on the weld seam formation at low welding velocity (v = 1.5 m/min) as well as on spatter formation during both, conventional welding techniques with center-gas application and modified techniques with additional side-gas. However, towards higher welding velocity (v = 3.0 m/min), the effect might be dominated by the weld pool dynamics itself. Eventually, a parameter for spatter control – the capillary widening ratio induced by the side-gas jet – was introduced. It was shown that the spatter quantity is dependent on this parameter. Overall, a wide process parameter region could be observed, where spattering was close to zero or could even be completely suppressed with deep penetration weld seams exhibiting good quality and partly showing strong bulge formations.

References

Abe, Y., Kawahito, Y., Nakamura, H., Mizutani, M., Katayama, S., 2014. Effect of reduced pressure atmosphere on weld geometry in partial penetration laser welding stainless and aluminum alloy with high power and high brightness laser, Science and Technology of Welding and Joining 19, p. 324-332.

Da Silva, A., Volpp, J., Frostevarg, J., Kaplan, A., 2021. Accelaration of metal drops in a laser beam, Applied Physics A 127, p. 1-13.

Fabbro, R., Slimani, S., Coste, F., Briand, F., Dlubak, B., Loisel, G., 2006. Experimental study of the dynamic coupling between the induced vapour plume and the meld pool for Nd-YAG CW laser welding, Journal of Physics D: Applied Physics 39, p. 394-400.

Fuhrich, T., 2005. Marangoni-Effekt beim Laserstrahltiefschweißen von Stahl. Herbert Utz Verlag, München.

Gao, M., Kawahito, Y., Kajii, S., 2017. Observation and understanding in laser welding of pure titanium at subatmospheric pressure, Optics Express 25, p. 13539-13548.

Heider, A., Sollinger, J., Abt, F., Boley, M., Weber, R., Graf, T., 2013. High-speed X-Ray analysis of spatter formation in laser welding of copper, Physics Procedia 41, p. 112-118.

Jarwitz, M., Lind, J., Weber, R., Graf, T., Influence of superimposed intensity distributions on the welding process and the spatter behaviour during laser welding of steel, Proc. of LiM., Munich.

Jovic, G., Bormann, A., Pröll, J., Böhm, S., 2019. Laser welding of thin stainless steel parts using modified side-gas application for control of spatter and weld shape, Proc. of LAMP - the 8th International Congress on Laser Advanced Materials Processing.

Jovic, G., Bormann, A., Pröll, J., Böhm, S., 2020. Laser welding with side-gas application and its impact on spatter formation and weld seam shape, Physics CIRP 94, p. 649-654.

Kamimuki, K., Inoue, T., Kouzou, Y., Muro, M., Nakabayashi, T., Matsunawa, A., 2002. Prevention of welding defect by side gas flow and its monitoring in continuous wave Nd:YAG laser welding, Journal of Laser Applications 14, p. 136-144.

Kaplan, A., Powell, J., 2011. Spatter in laser welding, Journal of Laser Applications 23, p. 032005.

Katayama, S., Abe, Y., Mizutani, M., Kawahito, Y., 2011. Deep Penetration Welding with High-Power Laser under Vacuum. Transactions of JWRI 40, p. 15-19.

Katayama, S., Kawahito, Y., 2009. Elucidation of Phenonema in High Power Fiber Laser Welding and Development of Prevention Procedures of Welding Defects, Proc. of SPIE 7195, p. 7195R1-R9.

Kawahito, Y., Kouki, N., Yousuke, U., Mizutani, M., Kouji, N., Hiroshi, K., Katayama, S., 2016. Relationship between melt flows based on three-dimensional X-ray transmission in-situ observation and spatter reduction by angle of incidence and defocusing distance in high-power, Quarterly Journal of the Japan Welding Society 34, p. 239-248.

Nakamura, H., Kawahito, Y., Katayama, S., 2015. Fundamental Study for the Relationship between Melt Flow and Spatter in High-Power Laser Welding of Pure Titanium, Transactions of JWRI 44, p. 27-32.

Ribic, B., Tsukamoto, S., Rai, R., Debroy, T., Role of surface-active elements during keyhole-mode laser welding, Journal of Physics D: Applied Physics 44, p. 458203

Schmidt, L., Hicketier, S., Schricker, K., Bergmann, J.-P., 2019. Low-spatter high speed welding by use of local shielding gas flows, Proc. of SPIE 10911, p. 109110V-1

Schmidt, L., Schricker, K., Bergmann, J.-P., Junger, C., 2020. Effect of Local Gas Flow in Full Penetraion Laser Beam Welding with High Welding Speeds, Applied Sciences 10, 1867, p. 1-19.

Sommer, M., Weberpals, J.-P., Heider, A., Prokop, M., Spatter occurrence when using laser beam oscillated welding for aluminum, Proc. of LiM, Munich.

Speker, N., Haug, P., Feuchtenbeiner, S., Hesse, T., Havrilla, D., 2018. BrightLine weld-spatter reduced high speed welding with disk lasers, Proc. of SPIE 10525, p. 10525C.

Su, Y., Li, Z., Mills, K.C., 2005. Equation to estimate the surface tension of stainless steels, Journal of Materials Science 40, p. 2201-2205.

Volpp, J., 2017. Dynamik und Stabilität der Dampfkapillare beim Laserstrahltiefschweißen, in “Strahltechnik Band 63”. BIAS Verlag, Bremen.

Weberpals, J.-P., 2010. Nutzen und Grenzen guter Fokussierbarkeit beim Laserstrahlschweißen. Herbert Utz Verlag, München.

Zhang, M., Chen, G., Zhou, Y., Li, S., Deng, H., 2013. Observation of spatter formation mechanisms in high-power fiber laser welding of thick plate, Applied Surface Science 280, p. 868-875.